Available online at www.sciencedirect.com
SCIENCE DIRECT®
Journal of Magnetic Resonance 165 (2003) 253–259
JMR Journal of Magnetic Resonance
www.elsevier.com/locate/jmr

Compensation of refocusing inefficiency with synchronized inversion sweep (CRISIS) in multiplicity-edited HSQC

Robert D. Boyer, Ross Johnson, and Krish Krishnamurthy*

Discovery Chemistry Research and Technologies, Lilly Research Laboratories, Indianapolis, IN 46285, USA

Received 11 March 2003; revised 6 August 2003

Communicated by Christian Griesinger

Abstract

Use of adiabatic pulses in broadband inversion and decoupling is well known. Replacement of the rectangular π pulses in the INEPT and rev-INEPT parts of the HSQC and gHSQC experiments with adiabatic pulses substantially improves the sensitivity of these experiments. However, modulation of cross peak intensity in multiplicity-edited HSQC or gHSQC experiments can be quite severe. These modulations arise during the multiplicity-editing periods due to the inefficient refocusing of the spin-echo caused by the mismatch of the echo delay with the one-bond coupling constant. These modulations (which we call echo modulations) are field strength (and hence spectral width) independent. Use of adiabatic pulses with the inversion sweep synchronized to the ^{1}H–^{13}C coupling constant range typically observed in a ^{13}C spectrum will provide substantial improvement in sensitivity. The inversion profile problems associated with rectangular π pulses can be moderately compensated by composite pulse schemes and these schemes could prove to be reasonable alternatives to adiabatic pulses. However, the adiabatic sweep provides a unique method to compensate the echo modulations for multiplicity-edited experiments. The origin and the compensation of refocusing inefficiency with synchronized inversion sweep (CRISIS) method to minimize these modulations is described.

Keywords: HSQC; Multiplicity-editing; Adiabatic pulse; Wurst2i pulse; Inversion sweep

1. Introduction

It is well recognized that the use of adiabatic pulses [1] is clearly a more efficient method for broadband inversion of nuclear spins over rectangular or composite pulses. Substantially improved broadband decoupling techniques with low radiofrequency intensities have been reported [2–16]. When used as a refocusing/inversion pulse, the offset dependent errors in chemical shift refocusing and in *J*-re(de)focusing efficiency, due to the longer sweep duration of the adiabatic pulses, have been addressed earlier [17–22]. The refocusing error can be corrected by applying the adiabatic pulse twice [22,23]. The second pulse now acts as a trim pulse and corrects for the phase error introduced by the first pulse [23]. Alternatively, one can employ a composite adiabatic pulse in the conventional way [20]. The *J*-refocusing error due to an adiabatic inversion pulse can either be corrected by applying a second pulse with the direction of the adiabatic sweep reversed, or taken advantage of in refocusing a range of coupling constants. These principles have been demonstrated earlier [22,24]. Kay and coworkers [25] exploited the linear relationship between ^{1}H–^{13}C scalar coupling and carbon chemical shift in optimizing the sweep rate of the adiabatic pulses during a heteronuclear spin-echo period for uniform and *J*-independent ^{13}C isotopic filtering.

Multiplicity-edited HSQC and gradient-HSQC (gHSQC) experiments [26–28] are very powerful tools in organic structure elucidation because they provide the heteronuclear [^{13}C] chemical shift and the multiplicity of the CH spin system in one experiment. Variations of these basic experiments to improve their sensitivity have been reported, particularly based on PEP (preservation of equivalent pathways) methodology [29,30]. In this

* Corresponding author. Fax: 1-317-276-5431.
E-mail address: krishk@lilly.com (K. Krishnamurthy).

1090-7807/$ - see front matter © 2003 Elsevier Inc. All rights reserved.
doi:10.1016/j.jmr.2003.08.009

report, we discuss the results of incorporating adiabatic pulses in the basic multiplicity-edited HSQC and gHSQC experiments and demonstrate the compensation of refocusing inefficiency with synchronized inversion sweep (CRISIS). The CRISIS leads to improved performance of multiplicity-edited HSQC and gHSQC experiments irrespective of the ^{13}C spectral width.

2. Results and discussion

The pulse sequences considered in this study are shown in Fig. 1. Sequence 1b is the same as 1a with all the ^{13}C inversion/refocusing π pulses replaced with adiabatic "pulse pairs" [22]. For convenience throughout this discussion, we use mult = 0 synonymously for multiplicity non-edited experiments and mult = 2 for multiplicity-edited experiments. The mult*pw90$_{(H)}$ represents the tip angle of the β pulse in sequences 1a and 1b.

The one-bond ^{13}C–^{1}H spin–spin coupling constants can typically range from 165 Hz for aromatic CH's to 125 Hz for aliphatic CH_3's. Figs. 2a–f illustrate the effect of J distribution on the intensity response in a gHSQCAD experiment. The profiles in Figs. 2a–f were generated with the δ value (and $\Delta/2$ value when mult = 2) changed systematically over ± 0.702 ms in 26 μs steps relative to the optimum δ values, in each case. This closely mimics the behavior of a $^{1}J_{CH}$ range of 180–120 Hz in an gHSQCAD experiment optimized for a nominal coupling constant of 146 Hz. The S_1 and S_2 pulses are wurst2i adiabatic shapes [11] of 400 μs duration and $B_{1(max)}$ of 14.9 kHz [31]. For all three spin systems with mult = 0, the profiles (Figs. 2a–c) show a good intensity response for the entire range of coupling constants. A small improvement in J-refocusing efficiency (in the INEPT and rev-INEPT portion of the pulse sequence) is achievable by matching the inversion sweep rate of the adiabatic pulse with the distribution of the one-bond coupling constant [25]. The profiles in Figs. 2d–f, where mult = 2, and $S_2 = S_1$, however, show severe compromises in intensity response when the actual coupling constants do not match with the delays chosen. These arise due to the refocusing inefficiency of the spin-echo during the Δ delay. The intensity response functions (ignoring homonuclear J, off-resonance and relaxation effects) for CH, CH_2, and CH_3 spin systems

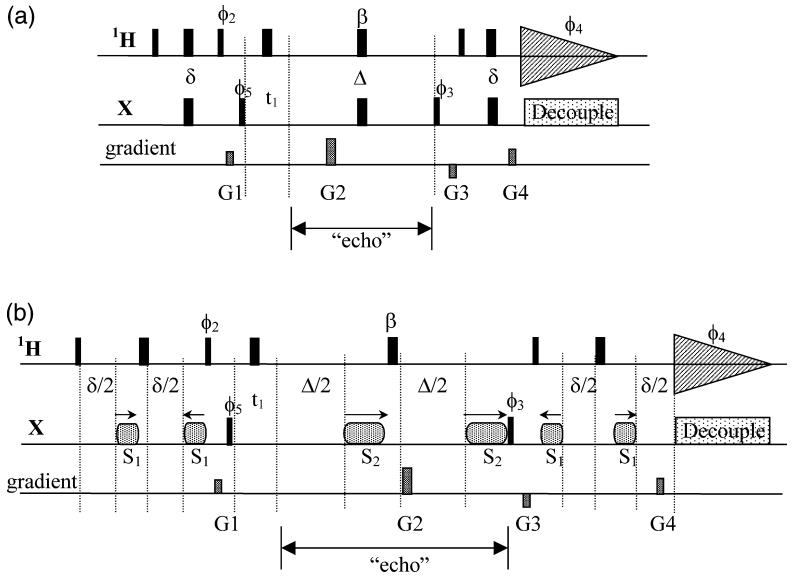

Fig. 1. Pulse sequences for non-gradient and gradient selected HSQC without (a) and with (b) adiabatic pulses. Thin and thick vertical lines represent 90° and 180° pulses, respectively. The adiabatic pulses (S_1 and S_2) are wurst2i shapes. The forward arrow represents a downfield to upfield sweep, while the reverse arrow represents an upfield to downfield sweep. The delay δ is set to $1/2J$. The basic phase cycling is $\phi_2 = y, y, -y, -y$; $\phi_3 = x, x, x, x, -x, -x, -x, -x$; $\phi_4 = x, -x, -x, x, -x, x, x, -x$; $\phi_5 = x, -x$. Phases not shown are along the x-axis. G1 and G3 are crusher gradients of amplitude 10 and 6 G/cm, respectively, with durations of 10 and 6 ms, respectively. For convenience, the non-gradient selected version of sequence 1a is referred to throughout this report as HSQC and the gradient selected version as gHSQC. Correspondingly, the two versions of sequence 1b will be referred to as HSQCAD and gHSQCAD ($S_1 = S_2$) or as CRISIS-HSQC and CRISIS-gHSQC ($S_1 \neq S_2$). For HSQC versions, the G2 and G4 gradients are turned off and quadrature selection in the t_1 dimension was achieved by a quadrature shift of ϕ_5 via the States-TPPI method. For gHSQC versions, the gradients G2 and G4 are set with a ratio of 4:1 (amplitudes of 10 and 5 G/cm and durations of 2 and 1 ms, respectively) for CH coherence selection and pure N- and P-type data are collected by inverting the sign of the G4 gradient, stored separately, and combined during processing to generate pure absorptive line shapes. For multiplicity-edited experiments, including CRISIS-HSQC and CRISIS-gHSQC, β is set to 180° and Δ is set to $1/J$. For gHSQC and gHSQCAD experiments without multiplicity-editing, β is set to 0° and Δ is set to twice the duration of the G1 gradient pulse and the gradient recovery delay. For HSQC and HSQCAD experiments without multiplicity-editing, all pulse, delay and gradient elements during the "echo" period are set to zero.

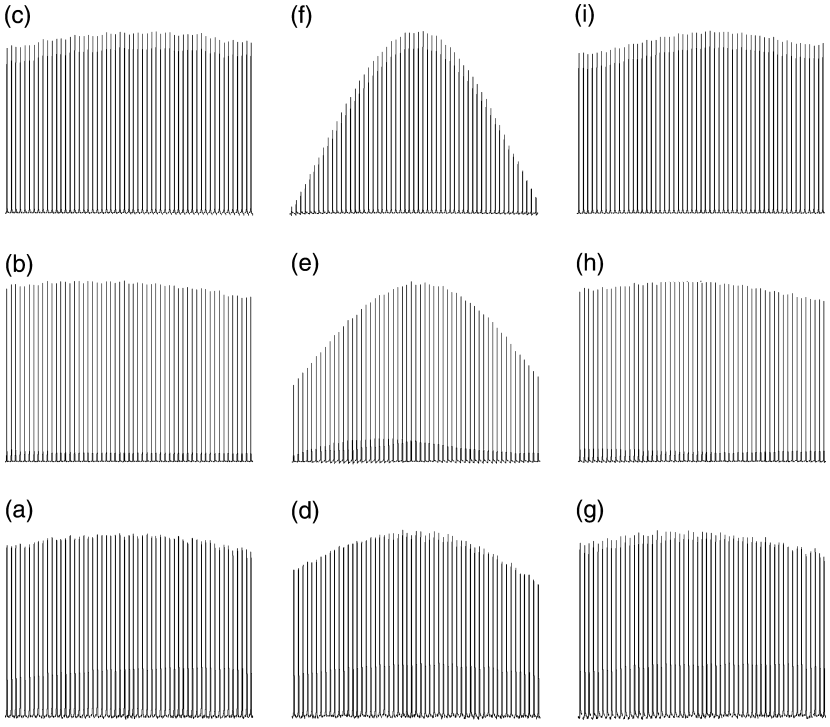

Fig. 2. First increment intensity profiles of gHSQCAD and CRISIS-gHSQC experiments using ^{13}C enriched samples of glucose (a,d, and g), glycine (b,e, and h), and methyl iodide (c,f, and i). Fifty-five spectra were generated (1 scan each) using sequence in Fig. 1b, with the δ (and $\Delta/2$) value systematically changed from +702 to −702 μs (around the optimum values of $1/2J$ in each case), in steps of 26 μs. The ^{13}C offset is simultaneously changed from +13,500 to −13,500 Hz (around the corresponding on-resonance frequencies) in steps of 500 Hz. A 400 μs wurst2i shape (51 kHz bandwidth) is used for the S_1 pulse. (a–c) gHSQCAD with mult = 0; (d–f) gHSQCAD with mult = 2, and $S_2 = S_1$; and (g–i) CRISIS-gHSQC with mult = 2 and a 2 ms wurst2i shape (34,500 Hz bandwidth) for the S_2 pulse.

in an edited gHSQC experiment can be described, based on Product Operator Formalism [32], as shown below:

$$\mathrm{CH} : \sin^2(\pi J\delta)\cos(\pi J\Delta), \tag{1}$$

$$\mathrm{CH_2} : 2\{\sin^2(\pi J\delta)[\cos^2(\pi J\Delta) - \sin^2(\pi J\Delta)]\}, \tag{2}$$

$$\underline{\mathrm{CH}}\mathrm{H}' : \sin^2(\pi J\delta)\cos(\pi J\Delta)\cos(\pi J'\Delta) - \sin(\pi J\delta) \times \sin(\pi J'\delta)\sin(\pi J\Delta)\sin(\pi J'\Delta), \tag{3}$$

$$\underline{\mathrm{CH}}\underline{\mathrm{H}}' : \sin^2(\pi J'\delta)\cos(\pi J'\Delta)\cos(\pi J\Delta) - \sin(\pi J'\delta) \times \sin(\pi J\delta)\sin(\pi J'\Delta)\sin(\pi J\Delta), \tag{4}$$

$$\mathrm{CH_3} : 3\{\sin^2(\pi J\delta)[\cos^3(\pi J\Delta) - 2\cos(\pi J\Delta) \times \sin^2(\pi J\Delta)]\}. \tag{5}$$

It should be noted that these echo modulations are independent of the offset and hence are equally applicable to a multiplicity-edited experiment run on a 300 MHz spectrometer or a 900 MHz spectrometer.

The intensity compromise in multiplicity-edited experiments is further illustrated using an equimolar mixture of three compounds **1–3**. This mixture has a wide range of both $^1J_{CH}$ (120–250 Hz) and carbon (protonated) chemical shifts (10–195 ppm) that are observed in typical organic structure fragments.

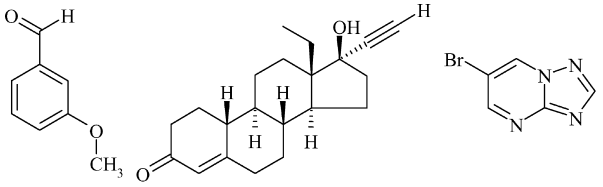

1 **2** **3**

In Fig. 3, ^1H–^{13}C 2D correlation contours and F_1 projections of HSQCAD spectra with mult = 0 (Fig. 3a) and mult = 2 (Fig. 3b) of the test sample are compared. The severe compromise in intensity of cross peaks is clearly evident throughout the spectrum in Fig. 3b. These effects are prominent for ^{13}C cross peaks with coupling constants substantially different from 146 Hz (the nominal value chosen, in these experiments), such as aldehyde and heteroaromatic cross peaks, and/or those with more than one directly attached proton. Synchronizing the inversion sweep rate of the S_2 pulses in these experiments to the distribution of the ^{13}C–^1H one-bond coupling (analogous to that reported earlier for isotopic filtering [25]) is highly desirable to compensate for the refocusing inefficiency.

There is a rough relationship between ^{13}C chemical shifts and the one-bond coupling constants and such

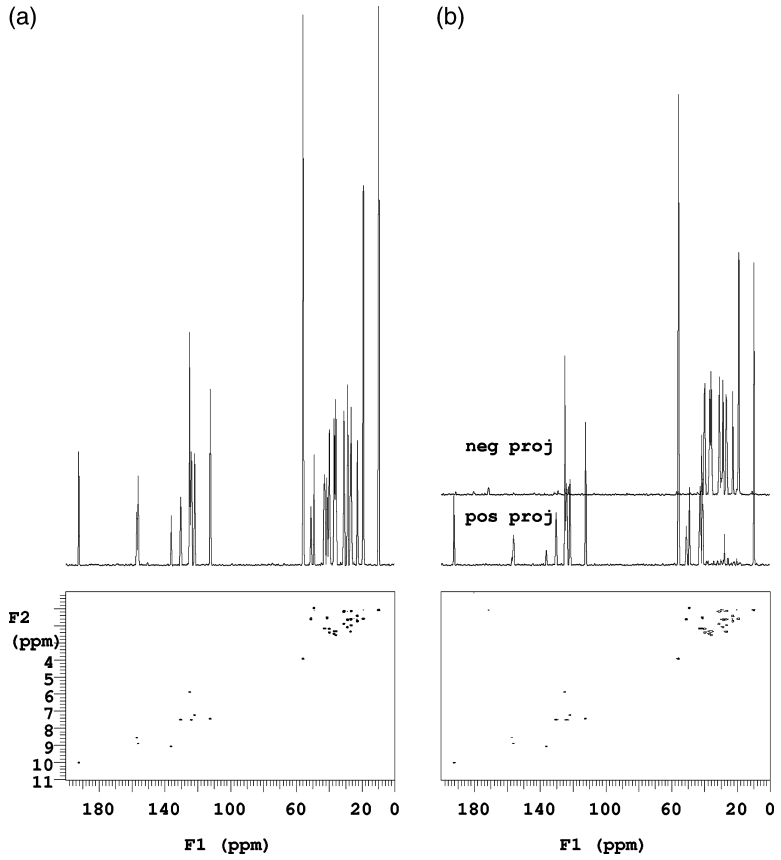

Fig. 3. Comparison of HSQCAD 2D spectra and their corresponding F_1 projections with (a) mult = 0 and (b) mult = 2 for the test sample, collected using the sequence in Fig. 1b.

correlations have been reported for proteins and RNA [25]. For organic structure fragments, except for acetylene and cyclopropyl carbons, we propose to use a value of 180 Hz coupling for a carbon at 180 ppm and a value of 120 Hz coupling for a carbon at 0 ppm, with a linear relationship between chemical shift and $1/2J$. This $\omega_{(c)}$–$^1J_{CH}$ relationship is depicted in Fig. 4 and is similar to that reported for proteins [25]. As shown earlier [22,24] the ideal inversion sweep duration, $\tau_{(opt)}$, for the S_2 pulses to match a range of coupling constants between J_{max} and J_{min} can be derived from the relationship:

$$\tau_{(opt)} = [J_{max} - J_{min}]/(*[J_{max}J_{min}])$$

The optimum inversion sweep duration ($\tau_{(opt)}$) for $J_{max} = 180$ Hz and $J_{min} = 120$ Hz, thus calculates to $\approx$700 μs. In the current proposal ($J_{max} = 180$ Hz at 180 ppm and $J_{min} = 120$ Hz at 0 ppm), this represents the optimum time difference between the inversion of a resonance at 90 ppm downfield and the one at 90 ppm upfield (i.e., +13,500 Hz and −13,500 Hz, respectively, for a 150 MHz ^{13}C resonance frequency). Fig. 5a shows the timing of the ±13,500 Hz inversions using wurst2i pulses (inversion bandwidth of 34,500 Hz) of varying duration. A 34,500 Hz (230 ppm) bandwidth was selected to include the aldehyde (typically >190 ppm) region. These plots were generated by simulating the z-magnetization trajectories of +13,500, 0, and −13,500 Hz resonances using Bloch simulations and determining the time when the magnetization crosses over from $+z$ to $-z$. As an approximation, the time required to achieve the spin inversion is neglected. From Fig. 5a, it is clear that a 2 ms wurst2i pulse satisfies

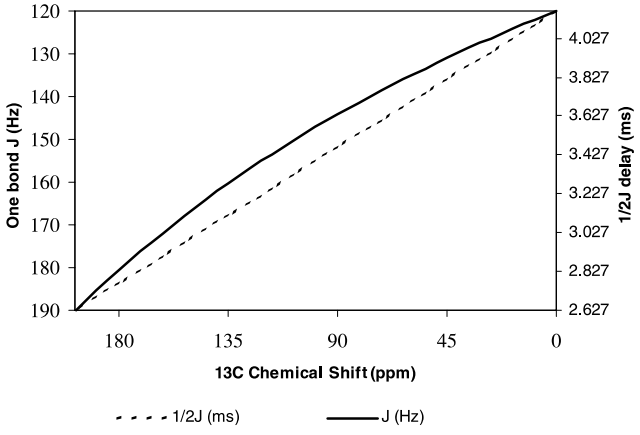

Fig. 4. Proposed relationship between ^{13}C chemical shift and one-bond ^{1}H–^{13}C coupling constant ($^1J_{CH}$) and optimum $\Delta/2$ delay ($1/2J$).

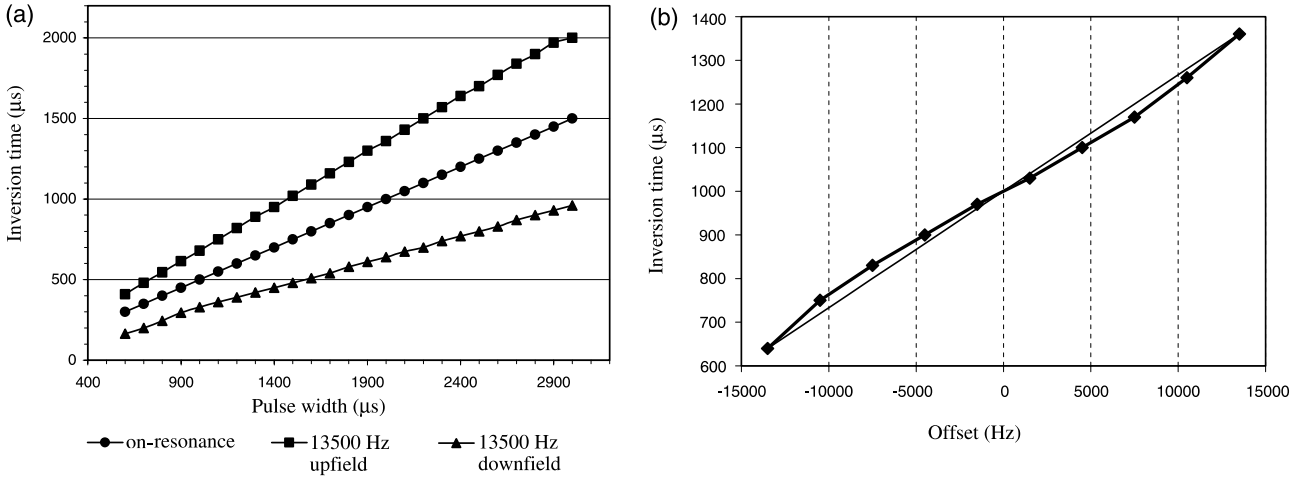

Fig. 5. (a) Inversion time of spins at +13,500 (downfield), −13,500 (upfield) Hz, and on-resonance spins as a function of wurst2i pulse duration. The inversion bandwidth for all the pulses is set to 34,500 Hz. The inversion time is defined as the instant at which the magnetization trajectory crosses over from $+z$ to $-z$. (b) A plot of the inversion time (the instant at which the magnetization trajectory crosses over from $+z$ to $-z$) of the spins as a function of their offset during a 2 ms wurst2i pulse.

the condition of 700 μs inversion sweep duration from +13,500 to −3500 Hz. Moreover, as plotted in Fig. 5b, the instant at which a given group of spins are inverted (when the magnetization trajectory crosses over from $+z$ to $-z$) shows a reasonably linear relationship to their offset. While the inversion times in Fig. 5b were generated using a wurst2i pulse of 2ms duration (34,500 Hz bandwidth) to mimic the behavior of 180–0 ppm ^{13}C resonances in a 600 MHz spectrometer, it is equally applicable to other field strengths as well. For example, a 2 ms wurst2i pulse with a 23000 Hz bandwidth will also show similar inversion times for ^{13}C resonances in a 400 MHz spectrometer.

Synchronization of the linear relationship between the inversion sweep and offset (as in Fig. 5b) with that proposed between $1/2J$ and the offset (as in Fig. 4) will result in the compensation of refocusing inefficiencies described in Eqs. (1)–(5) and observed in Figs. 2d–f. The CRISIS results are demonstrated in Figs. 2g–i. In each case, the profile was generated using the first increment gHSQCAD experiment using sequence 1b by simultaneously changing δ and Δ along with the ^{13}C offset across $\mp$13,500 Hz in steps of 500 Hz. Profiles in Figs. 2g–i were generated with mult = 2 and a 2 ms wurst2i S_2 pulse optimized for an inversion bandwidth of 34,500 Hz (230 ppm). The echo modulations introduced by refocusing inefficiencies (as shown in Figs. 2d–f) are now compensated in Figs. 2g–i. The CRISIS principle can be explained with three representative signals from the CH profile in Fig. 2g. (i) The first spectrum in Fig. 2g is run with δ and $\Delta/2$ set to 3.81 ms and the offset at −13,500 Hz from on-resonance (90 ppm downfield from the offset). Since S_2 is swept from low-field to high-field, the ^{13}C resonance is inverted 650 μs (see Fig. 5b) after the beginning of the S_2 pulse, i.e., 1350 μs before the end of the S_2 pulse. The effective dephasing of the heteronuclear J occurs during 3.11 ms (i.e., 700 μs *less* than $\Delta/2$), an optimum match for $1/2J$. (ii) The last spectrum in Fig. 2g is run with δ and $\Delta/2$ set to 2.41 ms and the offset at +13,500 from on-resonance (90 ppm upfield from the offset). This resonance is inverted 1350 μs after the beginning of the S_2 pulse. The effective dephasing of the heteronuclear J occurs during 3.11 ms (i.e., 700 μs *more* than $\Delta/2$), again, an optimum match for $1/2J$. (iii) The middle spectrum in Fig. 2g, on the other hand, is run with δ and $\Delta/2$ set to 3.11 ms and on-resonance. This ^{13}C resonance is inverted at the mid-point of the S_2 pulse and any dephasing of the heteronuclear coupling during first half of the pulse is compensated by the rephasing during the second half of the pulse. The effective dephasing of the heteronuclear J occurs during $\Delta/2$ period (3.11 ms), an optimum match for $1/2J$. Analogous explanations can be made for the profiles in Figs. 2h and i for the CH_2 and CH_3 spin systems. When the dephasing period (i.e., effective $\Delta/2$) matches $1/2J$, Eqs. (1), (2), and (5) reduce to $\sin^2(\pi J\delta)$. The CRISIS-gHSQC profiles in Figs. 2g–i, for all practical purposes, match the corresponding gHSQCAD (mult = 0) profiles in Figs. 2a–c.

In a practical situation, where there is a range of coupling constants involved and the δ and Δ are optimized for 146 Hz, the first intensity responses in Figs. 2g–i mimic the behavior of CH, CH_2, and CH_3 spins with a $^1J_{CH}$ of 180 Hz and resonating 90 ppm downfield from the ^{13}C offset, the middle intensity responses mimic those spins with a $^1J_{CH}$ of 146 Hz and resonating at the ^{13}C offset, while the last intensity responses mimic those spins with a $^1J_{CH}$ of 120 Hz and resonating 90 ppm upfield from the ^{13}C offset. The caveat in this approach is the basic hypothesis/assumption that a reasonably linear relationship (as depicted in Fig. 4) exists between

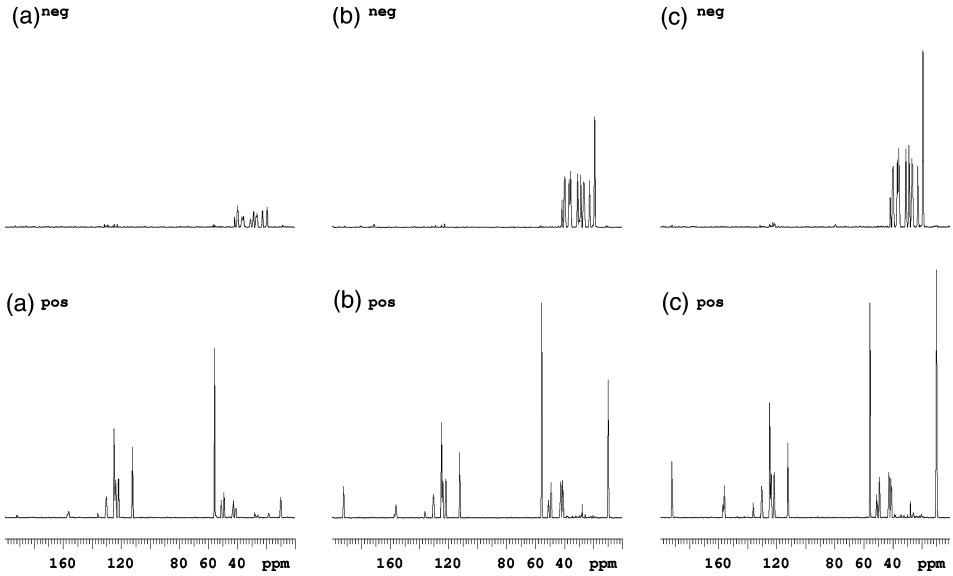

Fig. 6. Comparison of F_1 projections of multiplicity-edited (a) HSQC, (b) HSQCAD ($S_2 = S_1$), and (c) CRISIS-HSQC ($S_2 \neq S_1$) 2D spectra of the test sample mixture in $CDCl_3$. For convenience, the negative projections are plotted with the phase negated. A 400 μs wurst2i shape (51 kHz bandwidth) is used as the S_1 and S_2 pulses for the HSQCAD spectrum and as the S_1 pulse for the CRISIS-HSQC spectrum. A 2 ms wurst2i shape (230 ppm bandwidth) is used as the S_2 pulse for the CRISIS-HSQC spectrum.

chemical shift and the magnitude of $^1J_{CH}$. We tested the CRISIS effect using the test sample mixture, which exhibits a good range of $^1J_{CH}$ and δ_C. In Fig. 6, the F_1 projections of the multiplicity-edited 2D spectra are presented. The HSQC projections (Fig. 6a) show substantial compromise in intensity due to the combined effect of poor inversion bandwidth of the three π pulses and the echo modulation effect (as shown in Eqs. (1)–(5)) during multiplicity-editing. Peaks at the edges of the ^{13}C spectral width (such as the aldehyde peak and the methyl peak) have all but disappeared. In the HSQCAD projections (Fig. 6b), the effects due to the inversion bandwidth are compensated but those due to the echo modulations are not. In the CRISIS-HSQC projections (Fig. 6c), almost all peaks have increased sensitivity over Fig. 6b.

All the spectra in this study were run with the ^{13}C carrier frequency set at 90 ppm. The basic hypothesis/assumption of the linear relationship (as depicted in Fig. 4) between chemical shift and the magnitude of $^1J_{CH}$ is centered around 90 ppm. Hence, no adjustment to the Δ delay was needed for the CRISIS-HSQC experiment when using the 2 ms S_2 pulse, if the ^{13}C carrier frequency is set at 90 ppm. However, when spectra are run with the ^{13}C carrier frequency not set at 90 ppm, one can use the same 2 ms S_2 pulse, after applying a small correction (Δ_c) to Δ, where

$$\Delta_c = (90\text{-}\delta_{offset}) * (700/180)\ \mu s$$

and δ_{offset} is the chemical shift at the ^{13}C offset. The factor 700/180 comes from the derived relationship that 700 μs is the optimum inversion sweep time across 180 ppm. Alternately, one could use frequency shifted S_2 pulses (shifted by 90-δ_{offset}) to achieve the same result.

3. Experimental

All spectra were recorded at 25 °C on a Varian UnityINOVA 600 MHz NMR spectrometer equipped with the Programmable Pulse Modulator in the X channel, a gradient accessory and a 3 mm $^1H\{X\}$ indirect detection probe. All shaped pulses were generated using the Pandora's Box pulse shaping program [33] and all Bloch simulations were done using the Pulsetool program, both available as part of the Varian NMR software. The gradients are rectangular shaped. The ^1H 90° pulse width is 6 μs and the non-selective ^{13}C 90° pulse width is 12 μs. The S_1 and S_2 pulses were wurst2i adiabatic sweeps. For all spectra/profiles in Figs. 2,3,6b and c the bandwidth for the S_1 pulse is 51 kHz (an arbitrary 15% more than a 300 ppm ^{13}C width) and the duration is 400 μs. For profiles in Figs. 2a–f and the spectra and projections in Figs. 3b and 6b, $S_2 = S_1$. For the profiles in Figs. 2g–i and the spectra in Fig. 6c, the bandwidth for the S_2 pulse is 34.5 kHz (230 ppm) and the duration is 2 ms.

The profiles in Fig. 2 were generated using ^{13}C enriched samples of glucose [C_1–^{13}C], glycine [C_2–^{13}C], and methyl iodide. The glucose and glycine are 20 mM solutions in D_2O while the methyl iodide is a 2% solution in $CDCl_3$. The ^1H chemical shifts of glucose (α isomer), glycine, and methyl iodide are 4.52, 3.43, and 2.16 ppm, respectively. The ^{13}C chemical shifts of glu-

cose (α isomer), glycine, and methyl iodide are 94, 37, and −23 ppm, respectively. The measured $^1J_{CH}$ values for glucose (α isomer), glycine, and methyl iodide are 161, 143, and 151 Hz, respectively. The spectra in Figs. 3 and 6 were generated using a 20 mM solution of the test sample (a 1:1:1 mixture of **1–3**) in $CDCl_3$ using a nominal $^1J_{CH}$ of 146 Hz. Four scans of 2800 complex points were collected for each of the 128 t_1 increments. A 230 ppm ^{13}C (F_1) spectral width centered around 90 ppm was used. A relaxation delay of 1 s was used prior to each scan. A TANGO [34] pulse followed by a crusher gradient of 10 G/cm for a duration of 4 ms followed the relaxation delay and preceded the first proton pulse to aid suppression of ^{12}C–^1H. The S_1 pulse is used in place of the ^{13}C π pulse in the TANGO pulse train, as well. The total acquisition time for each of the 2D spectra was ~20 min. All 1D spectra were processed with 4× zero filling after applying an unshifted gaussian window. All 2D data were processed with an unshifted gaussian window function in both F_1 and F_2 dimensions followed by Fourier transformation. The t_1 interferograms were linear predicted to 4× the number of increments collected, prior to multiplication with the window function. The spectra were transformed with 2048 × 2048 complex points.

4. Conclusion

The echo modulation of cross peak intensity in multiplicity-edited HSQC or gHSQC experiments can be quite severe. These modulations are caused by refocusing inefficiency of the spin-echo and are field strength (and hence spectral width) independent. Compensation of refocusing inefficiency by synchronizing the inversion sweep (CRISIS) with the $^1J_{CH}$ range (typically observed in ^{13}C spectrum) will provide substantial improvement in the sensitivity. While inversion profile problems associated with rectangular π pulses can be compensated to some extent by composite pulse schemes [35] and that these schemes could prove to be reasonable alternatives to adiabatic pulses at least at moderate field strengths, the echo modulation problem in multiplicity-edited experiments, described in this report, cannot be compensated with composite pulse schemes. CRISIS provides a unique solution to compensate the echo modulation problem. The 2 ms wurst2i pulse with an inversion bandwidth of 230 ppm conveniently satisfies the 700 μs inversion sweep timing needed to compensate a 180–120 Hz coupling distribution across 180–0 ppm. While the proposed chemical shift to coupling constant relationship is still hypothetical, it is quite useful in improving the sensitivity of the experiment, as demonstrated using the test mixture.

References

[1] A. Abragam, The Principles of Nuclear Magnetism, Oxford University Press, Oxford, 1961.
[2] J.M. Böhlen, J. Bodenhausen, J. Magn. Reson. 90 (1990) 183.
[3] J.M. Böhlen, J. Bodenhausen, J. Magn. Reson. A 102 (1993) 293.
[4] T. Jujiwara, T. Anai, J. Kurihara, K. Nagayama, J. Magn. Reson. A 104 (1993) 103.
[5] Z. Starčuk Jr., K. Bartušek, Z. Starčuk, J. Magn. Reson. A 107 (1994) 24.
[6] M.R. Bendall, J. Magn. Reson. A 112 (1995) 126.
[7] Ē. Kupče, R. Freeman, J. Magn. Reson. A 115 (1995) 273.
[8] R. Fu, G. Bodenhausen, Chem. Phys. Lett. 245 (1995) 415.
[9] Ē. Kupče, R. Freeman, J. Magn. Reson. A 117 (1995) 246.
[10] R. Fu, G. Bodenhausen, J. Magn. Reson. A 117 (1995) 324.
[11] Ē. Kupče, R. Freeman, J. Magn. Reson. A 118 (1996) 299.
[12] R. Fu, G. Bodenhausen, J. Magn. Reson. A 119 (1996) 129.
[13] Ē. Kupče, R. Freeman, Chem. Phys. Lett. 250 (1996) 523.
[14] M.R. Bendall, T.E. Skinner, J. Magn. Reson. A 120 (1996) 77.
[15] A. Tannus, M. Garwood, J. Magn. Reson. A 120 (1996) 133.
[16] Ē. Kupče, R. Freeman, G. Wider, K. Wüthrich, J. Magn. Reson. A 120 (1996) 264.
[17] S. Connolly, G. Glover, D. Nishimura, A. Macovski, Magn. Reson. Med. 18 (1991) 28.
[18] V.L. Ermakov, J.M. Böhlen, G. Bodenhausen, J. Magn. Reson. A 103 (1993) 226.
[19] T.-L. Hwang, A.J. Shaka, J. Magn. Reson. A 112 (1995) 275.
[20] T.-L. Hwang, P.C.L. van Zijl, M. Garwood, J. Magn. Reson. 124 (1997) 150.
[21] K. Ogura, H. Terasawa, F. Inagaki, J. Magn. Reson. B 112 (1996) 63.
[22] Ē. Kupče, R. Freeman, J. Magn. Reson. 127 (1997) 36.
[23] K. Stott, J. Stonehouse, J. Keeler, T.-L. Hwang, A.J. Shaka, J. Am. Chem. Soc. 117 (1995) 4199.
[24] Ē. Kupče, Methods Enzymol. 338 (2001) 82.
[25] C. Zwahlen, P. Legault, S.J.F. Vincent, J. Greeenblatt, R. Konrat, L.E. Kay, J. Am. Chem. Soc. 119 (1997) 6711.
[26] G. Bodenhausen, D.J. Ruben, Chem. Phys. Lett. 69 (1980) 185.
[27] G.W. Vuister, R. Böelens, R. Kaptein, R.E. Hurd, B. John, P.C.M. Van Zijl, J. Am. Chem. Soc. 113 (1991) 9688.
[28] A. Bax, S. Pochapsky, J. Magn. Reson. 99 (1992) 638.
[29] J. Cavanagh, M. Rance, Annu. Rep. NMR Spectrosc. 27 (1993) 1.
[30] A.G. Palmer, J. Cavanagh, P.E. Wright, M. Rance, J. Magn. Reson. 93 (1991) 151.
[31] The 400 μs wurst2i pulse of $B_{1(max)} = 14.9$ kHz is swept across +/−25.5 kHz achieves an effective inversion [>95% based on Block simulation and experimental inversion profile] across 300 ppm [45 kHz] bandwidth in a 600 MHz spectrometer.
[32] O.W. Sørensen, G. Eich, M.H. Levitt, G. Bodenhausen, R.R. Ernst, Prog. NMR Spectrosc. 16 (1983) 163.
[33] Ē. Kupče, R. Freeman, J. Magn. Reson. A 105 (1993) 234.
[34] S. Wimperis, R. Freeman, J. Magn. Reson. 58 (1984) 348.
[35] R. Freeman, S.P. Kempsell, M.H. Levitt, J. Magn. Reson. 38 (1980) 453.